European Cells and Materials Vol.57 2026 (pages 66–81) DOI: 10.22203/eCM.v057a03 ISSN 1473-2262

Original Article

INHALABLE BIONIC NANOPARTICLE VACCINE MIMICKING PULMONARY SURFACTANT ENHANCES ANTI-TUBERCULOSIS IMMUNITY

Yanqiu Wu[1,§], Weifeng Ma[4,§], Han Duan[4], Xinting Fu[4], Jiamei Wang[5], Chunhua Yang[6], Qin Gu[2], Yue Jia[3], Yunlong Zhang[7], Fei Ma[3], Zihui Wei[4], Bohua Ren[2], Qinqin Wang[2], Yuehua Hei[2], Qiang Ma[1,*] and Bin Li[2,3,*]

[1]Guangdong Provincial Key Laboratory of Immune Regulation and Immunotherapy, School of Laboratory Medicine and Biotechnology, Southern Medical University, 510000 Guangzhou, Guangdong, China
[2]School of Inspection, Ningxia Medical University, 750004 Yinchuan, Ningxia, China
[3]School of Basic Medical Sciences, Ningxia Medical University, 750004 Yinchuan, Ningxia, China
[4]Department of Microbiology, School of Public Health, Southern Medical University (Guangdong Provincial Key Laboratory of Tropical Disease Research), 510515 Guangzhou, Guangdong, China
[5]Institute for Engineering Medicine, Kunming Medical University, 650500 Kunming, Yunnan, China
[6]Institute for Biomedical Sciences, Georgia State University, Atlanta, GA 30303, USA
[7]Department of Critical Care Medicine & Department of Emergency, Renmin Hospital of Wuhan University, 430060 Wuhan, Hubei, China
[§]These authors contributed equally.

Abstract

Background: Tuberculosis (TB), an infectious disease caused by *Mycobacterium tuberculosis* (M.tb), remains a formidable global public health threat. The currently available Bacillus Calmette-Guérin (BCG) vaccine, while effective in children, provides inadequate protection for adults, highlighting an urgent need for novel vaccine development. **Methods:** This study constructed an inhalable biomimetic nanoparticle vaccine, designated ECQ@PS-LPs. The vaccine utilizes liposomes that mimic natural pulmonary surfactant as a carrier to co-encapsulate two key TB antigens, ESAT-6 and CFP-10, along with the immunoadjuvant QS-21. Following intranasal administration in mice, immune responses and protective efficacy were evaluated. Using one-way ANOVA with post-hoc testing, statistical significance was defined as $*p < 0.05$, $**p < 0.01$ and $***p < 0.001$. **Results:** The ECQ@PS-LPs vaccine effectively breached the alveolar surfactant barrier, significantly enhancing uptake by antigen-presenting cells. This triggered a robust multidimensional immune response, including potent cellular immunity (characterized by Th1 and Th17 responses), systemic humoral immunity (indicated by IgG production), and strong mucosal immunity (evidenced by sIgA). Furthermore, the vaccine induced durable immune memory, marked by the generation of tissue-resident memory T cells (TRM) and central memory T cells (TCM). In a M.tb challenge model, ECQ@PS-LPs conferred a level of protection comparable to the BCG vaccine and elicited a superior mucosal immune response. The vaccine formulation also demonstrated a simple preparation process and favorable biological safety profile. **Conclusions:** ECQ@PS-LPs represents a promising inhalable candidate vaccine for TB. It effectively induces comprehensive and persistent immune protection, particularly at the mucosal site, offering a novel and strategic direction for preventing TB in adults.

Keywords: Tuberculosis, biomimetic nanovaccine, alveolar surfactant-mimicking, cellular immunity.

***Address for correspondence**: Qiang Ma, Guangdong Provincial Key Laboratory of Immune Regulation and Immunotherapy, School of Laboratory Medicine and Biotechnology, Southern Medical University, 510000 Guangzhou, Guangdong, China. E-mail: Mq@smu.edu.cn; Bin Li, School of Inspection, Ningxia Medical University, 750004 Yinchuan, Ningxia, China; School of Basic Medical Sciences, Ningxia Medical University, 750004 Yinchuan, Ningxia, China. E-mail: libin63@alumni.sysu.edu.cn.

Introduction

Tuberculosis (TB), an ancient disease with origins dating back tens of thousands of years [1], is caused by *Mycobacterium tuberculosis* (M.tb). The bacterium is primarily spread via airborne droplets and most commonly infects the lungs, causing pulmonary TB. In some instances, the infection can spread to other parts of the body, such as the lymph nodes, bones, kidneys, and brain; this form is classified as extrapulmonary TB [2]. TB remains one of the world's leading infectious causes of morbidity and mortality [3]. It is classified by the World Health Organization (WHO), alongside HIV/AIDS and malaria, as one of the three major infectious diseases [4]. Although TB control strategies have come a long way, great challenges remain. One of the key problems is that M.tb grows extremely well and can remain dormant in the host body, which is difficult to remove [5]. The efficacy of most antibiotics is limited to actively replicating bacilli, which dictates the need for lengthy treatment regimens to fully eliminate the pathogen [6]. This paradigm of care places a premium on strict patient adherence—a variable that also impedes the clinical development of new therapeutic agents. Moreover, the situation is exacerbated by the steadily increasing global incidence of multidrug-resistant (MDR), extensively drug-resistant (XDR) TB [7]. Although the Bacillus Calmette-Guérin (BCG) vaccine is the only widely implemented TB vaccine and provides relatively good protection in pediatric populations [8], this protection does not extend to adults [9]. This limitation underscores the imperative to develop novel preventive vaccines, which are crucial for controlling the spread of drug-resistant strains, reducing TB incidence, and interrupting disease transmission at its source [10].

To date, numerous types of TB vaccines have been developed, including subunit vaccines [11], viral vector vaccines [12], mRNA vaccines [13], and others. Nanomaterials also play a crucial role in the research and application of modern vaccines [14–17]. Because bionic nanovaccine [18] exhibit exceptional biocompatibility and safety, significantly reducing potential biotoxicity associated with traditional nanomaterials and enhancing vaccine safety. Furthermore, nanovaccine possess potent immune-activating efficacy [19], thanks to their size facilitating efficient phagocytosis and processing by antigen-presenting cells (APCs).

We developed liposomes that mimic pulmonary surfactant (PS) and co-encapsulated two M.tb-specific antigens (ESAT-6 and CFP-10) together [20] with the adjuvant QS-21, forming a biomimetic nanovaccine designated ECQ@PS-LPs (Fig. 1**A**). ESAT-6 and CFP-10 are highly expressed in the early stage after bacterial infection of the host, and can be quickly recognized by the immune system, which helps to activate protective immunity in the early stage and block the latency and spread of pathogens, QS-21 (also known as saponin-8), a plant saponin derived from the bark of Quillaja saponaria, enhances immune responses through multiple mechanisms [21]. These include promoting dendritic cell activation; balancing Th1/Th2 responses, stimulating cytokine secretion (e.g., IFN-γ) [21]. PS-LPs by virtue of its biomimetic PS-mimicking system, ECQ@PS-LPs efficiently penetrates the pulmonary surfactant barrier and is taken up by antigen-presenting cells (APCs). This process, which crucially maintains the structural integrity of the nanovesicles, initiates a cascade of immune responses (Fig. 1**B**). The ECQ@PS-LPs nanovaccine particles measure approximately 200 nm in size, a dimension that facilitates easier phagocytosis and processing by antigen-presenting cells (APCs). Compared to conventional intramuscular injections, inhaled vaccines [22] enable broader mucosal coverage and can elicit robust immune protection with lower antigen doses. Given the primary airborne transmission of TB, inhalable vaccines [23] can directly bolster immune defenses at the initial site of infection. Intranasal administration of ECQ@PS-LPs effectively induced Th1 versus Th17 cellular immune responses in a mouse model [24]. Among them, Th1 cells are particularly critical in TB immunity, mainly through cytokines such as IFN-γ: on the one hand, IFN-γ can activate macrophages and enhance their ability to kill intracellular pathogens; On the other hand, it is also an important signaling molecule for the formation and maintenance of granuloma, thus helping to limit the spread of M.tb. Th17 cells contribute to host defense by recruiting neutrophils to control bacterial dissemination in early infection, strengthening mucosal barrier function, and acting in synergy with Th1 responses. In parallel, the frequencies of tissue-resident memory T cells (TRM) [25] and central memory T cells (TCM) [26] were notably elevated in the spleen. TRM [25] cells are strategically localized in barrier tissues (e.g., lungs, intestines) and are non-circulatory, enabling them to constitute a first line of defense. Following antigen re-exposure, these cells are immediately activated to exert effector functions, providing a rapid response that does not depend on recruitment or proliferation. TCM cells, on the other hand, recirculate through the blood, lymphatic system, and secondary lymphoid organs such as the spleen. When re-exposed to the same pathogen, TCM cells undergo rapid proliferation and differentiation into a substantial army of effector T cells, which are responsible for mediating systemic, whole-body immunity. These cells function as the principal reservoir for lifelong immune memory, with the ability to persist for decades. Furthermore, ECQ@PS-LPs induced potent mucosal immunity in the lungs, characterized by high titers of antigen-specific secretory IgA (sIgA), which established a primary defensive barrier against M.tb (Fig. 1**B**). Theoretically, mucosal vaccines can simultaneously provide localized protection, systemic immunity, and—through lymphocyte homing to distant sites—extended mucosal defense.

In conclusion, the inhalable vaccine platform we built has shown multi-dimensional potential in the field of TB

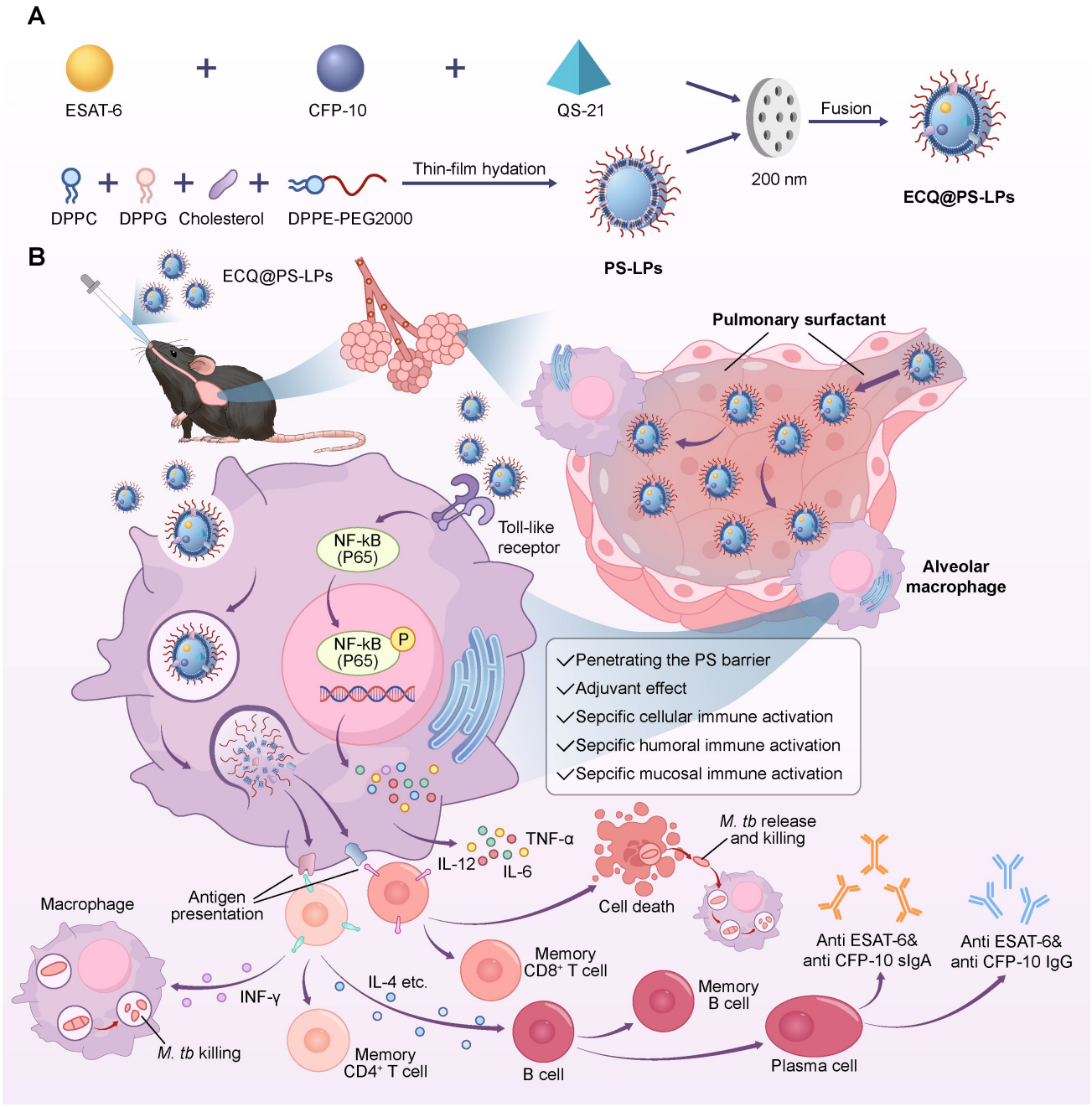

Fig. 1. Schematic diagram of the preparation process and protective mechanism of ECQ@PS-LPs. (**A**) Schematic diagram illustrating the preparation of ECQ@PS-LPs. (**B**) Schematic representation of the penetration, immune activation, and protective effects of ECQ@PS-LPs against respiratory TB transmission. (Drawing software: Adobe Illustrator 2025)

prevention: it can not only effectively induce strong cellular and mucosal immune responses, but also form stable and long-lasting immune memory. Compared with the M72/AS01E [11] and other protein subunit vaccines currently in the clinical stage, the platform uses a bionic lipoprotein particle delivery system, which has a significantly longer residence time in the lungs, and can simultaneously activate antigen-specific Th1, Th17 and cytotoxic T cell response, this multi-polarized immune feature is better than the existing technical route based on humoral immunity. In the research and development trend of mucosal vaccines [27] that has attracted much attention in recent years, this platform has broken through the limitation that traditional injection vaccines are difficult to establish an immune barrier at the infection portal through the "inhalation-mucosa-systemic" three-level immune activation mode. The efficient delivery and immune regulation capabilities demonstrated by this platform provide a new strategy for overcoming bottlenecks such as uneven protection and short memory maintenance in the current research

and development of TB vaccines, especially for the development of the next generation of TB vaccines that can both prevent infection and block transmission. Vaccines provide key experimental basis and feasible transformation paths.

Materials and Methods

Materials

The lipids utilized for the preparation of ECQ@PS-LPs were sourced from Avanti Polar Lipids, which included 1,2-dipalmitoyl-sn-glycero-3-phosphocholine (DPPC) (Cat# LP-R4-057), 1,2-dipalmitoyl-sn-glycero-3-phosphoglycerol (DPPG) (Cat# LP-R4-016-1), and 1,2-distearoyl-sn-glycero-3-phosphoethanolamine-N-[methoxy (polyethylene glycol)-2000] (DSPE-PEG2000) (Cat# R-0041), which were purchased from Ruixibio, China. Cholesterol (Cas# 57-88-5) were obtained from Sigma-Aldrich, Germany. ESAT-6 (Cat# ab124574) was purchased from Abcam, China. CFP-10 (Cat# DRA28) from NOVOPROTEIN, China; and QS-21(Cas# 141256-04-4) from GLPBIO, China. Dulbecco's modified Eagle medium (DMEM; Cat# 21013024), fetal bovine serum (FBS; Cat# 10270106), penicillin/streptomycin (Cat# 15140122), glutamine, were purchased from Gibco (USA). 1.5 mL centrifuge tube (Cat# 615001), cell culture dishes (Cat# 704002), and glass-bottom cell dishes (Cat# 801002) were supplied by NEST Biotechnology (China). 1,1-Dioctadecyl-3,3,3,3- tetramethylindotricarbocyanine iodide (DIR; Cat# D9320) and red blood cell lysis buffer (Cat# R1010) were obtained from Beijing Solarbio Science & Technology (China). The SurePAGE Bis-Tris 12% 12-well gel (Cat# LK305) was from EpiZyme (China). Cell proliferation assay kit (Cat# CA1210) and hematoxylin–eosin staining kit (Cat# G1121) were purchased from Beijing Solarbio (China). The bicinchoninic acid (BCA) protein assay kit (Cat# KGP902) and DAPI staining solution (Cat# KGA1808) were supplied by KeyGEN Biotechnology (China). Coomassie Brilliant Blue staining solution (Cat# P0004M) was sourced from Beyotime (China). Collagenase V (Cat# C9263) was purchased from Sigma-Aldrich (Germany). Polycarbonate filters (800, 400, and 200 nm; Cat# PC190800, PC190400, PC190200) were obtained from MORGEC (China). Flow cytometry antibodies were purchased from eBioscience (USA); detailed information is provided in **Supplementary Table 1**.

Cell Culture

The murine macrophage cell line RAW 264.7 (ATCC® TIB-71™) was acquired from the Shanghai Cell Bank of the Chinese Academy of Sciences. The cells were cultured in Dulbecco's Modified Eagle Medium (DMEM) containing 10% heat-inactivated fetal bovine serum (FBS), 50 U/mL penicillin, and 50 μg/mL streptomycin. All cultures were maintained in a sterile, humidified atmosphere of 5% CO_2 and 95% air at 37 °C.

Preparation and Characterization of ECQ@PS-LPs

A lipid mixture of DPPC, DPPG, DSPE-PEG2000, and cholesterol at a mass ratio of 10:1:1:1 (with DPPC fixed at 1 mg) was dissolved in chloroform. The solution was subjected to rotary evaporation at 50 °C under vacuum using a condensation circulation pump to form a thin, light-yellow lipid film. Subsequently, 1 mL of PBS containing 15 μg QS-21, 4 μg ESAT-6, and 4 μg CFP-10 was added to hydrate the film. The mixture was thoroughly vortexed and homogenized in an ice-water bath, followed by sequential extrusion through 800 nm, 400 nm, and 200 nm polycarbonate membranes (15 passes per membrane) to obtain ECQ@PS-LPs.

The particle size and zeta potential of both plain PS-LPs and ECQ@PS-LPs were measured using a nanoparticle analyzer (Litesizer 500, Anton Paar). The morphology and structure of the liposomes were characterized by transmission electron microscopy (JEM-6510A, JEOL).

SDS-PAGE

Load an 12% 12-well gel with Marker, PS-LPs, CFP-10, ESAT-6, and ECQ@PS-LPs. 60 V, 30 min; 120 V, 2 h. Stain with Biogenet Coomassie Brilliant Blue for 3–60 min, then wash with ddH_2O until desired results are achieved.

Mouse Immunization

The study used a completely randomized experimental design. The experimental groups included G1 (PBS), G2 (free ESAT-6+CFP-10), G3 (free ESAT-6 + CFP-10 + QS-21), G4 (BCG SC), G5 (ECQ@PS-LPs). A single 6–8-week-old female C57BL/6 mouse (weight, 16–25 g; purchased from the Guangdong Medical Laboratory Animal Center) served as the experimental unit. Three biological replicates were set for each group, using a total of 15 mice, each administered with twice vaccine. All adaptively housed in SPF-grade animal facilities under: 20–22 °C, 30–70% humidity, 12 h light-dark cycle. In good health and free of infection by specific pathogens, all were wild type without any previous treatment, all are determined in advance. Before the experiment, they were fed adaptively in the facility for a week. All animal procedures were approved by the Ethics Committee of Ningxia Medical University and performed following the relevant ethical guidelines (Approval No.: 2024-G048). Mice were anesthetized with tribromoethanol. Each group was instilled vaccine suspension by nasal inhalation on day 0 and day 28. Each mouse, regardless of body weight, was given 30 μL of antigen and adjuvant suspension containing ESAT-6 (4 μg), CFP-10 (4 μg) and QS-21 (15 μg). Group G4 subcutaneous inoculation 1×10^6 CFU BCG. Mice were sacrificed on day 31, and their spleens, lung and serum were taken for flow cytometry and ELISA analysis. The purpose of instillation on day 0 is to initiate a primary immune response, while day 28 is to stimulate a strong re-immune response and immune memory. Mice were sacrificed for testing on day 31 to facil-

itate testing when positive indicators were most evident. All operations were completed in the experimental operation room of the animal room. Before the experiment, the random assignment sequence was generated by the R language (v4.2.0) (R Foundation for Statistical Computing, Vienna, Austria), and the cage position on the feeding rack was rearranged according to the random sequence to control the potential environmental confounding factor of "cage position". In the implementation process, a three-blind design is adopted: only the project leader has the packet key; Operators know the blind coding but do not know the actual group correspondence; Results Evaluators were completely unaware of grouping assignments; In the data analysis stage, blind codes are used during data collation and preliminary analysis, and blindness is only unblinding before final statistical inference. The main observation indexes were the changes of Th1, Th17, TCM, TRM-related immune indexes and the expression of specific IgG and sIgA. Data analysis was performed using one-way ANOVA with post hoc tests, and data were presented as mean ± SD, $*p < 0.05$, $**p < 0.01$, $***p < 0.001$. All datasets met the ANOVA premise assumptions (using software: Prism 10). In view of the fact that this study is an exploratory pre-experiment, the sample size is set by similar preliminary studies in the reference field, no prior sample size calculation is performed, and the effect size and confidence interval are not reported due to the small sample size. All included healthy female C57 mice completed the experimental pipeline, and individuals with no technical reasons (anesthesia accidents, dosing errors, etc.) or who developed severe disease/injury unrelated to experimental treatment were excluded. In all behavioral and histological analyses, the final n-value was 3 for each group.

Challenge With Bacillus Calmette-Guérin (BCG) Strain

To evaluate the protective effect of different immunization preparations, we infected 3 mice in each group with about 100 CFU of BCG via the respiratory tract using aerosols at known concentrations 6 weeks after the last immunization. One month after infection, mouse lung tissue was removed and placed in PBS with 0.05% Tween 80 for homogenization. The homogenate was coated on 7H10 agar plates supplemented with 10% OADC nutritional additive and cultured at 37 °C for 30 days, and the number of bacterial colony forming units (CFU) per organ was counted. At the same time, lung tissue was taken for follow-up analysis.

Flow Cytometry

Single-cell suspensions were prepared from the harvested lung and spleen tissues and stimulate with specific antigens, incubating overnight, centrifuging to obtain cells, for subsequent analytical procedures (competing for adaptive immunity). In brief, approximately 30 mg of lung tissue was mechanically dissociated into fine fragments using a scalpel. Tissue was then digested with V-type collagenase (37 °C, 30 min). The cell digest was sequentially filtered through a 70 μm cell strainer and subjected to red blood cell lysis to remove contaminating erythrocytes. The cell pellet was washed 2–3 times with cold PBS. To block non-specific binding, the cells were resuspended in PBS containing 1% BSA and incubated on ice for 30 minutes. After washing again with PBS to remove the blocking buffer, the cells were stained with the appropriate fluorochrome-conjugated antibodies for 30 minutes at 4 °C in the dark. Unbound antibodies were removed by an additional PBS wash. For intracellular targets, the cells were then fixed and permeabilized using a dedicated buffer solution according to the manufacturer's instructions, which included centrifugation and wash steps. Stained samples were ultimately acquired on a flow cytometer, and the resulting data were analyzed with FlowJo software.

Enzyme-Linked Immunosorbent Assay (ELISA)

Indirect ELISA was performed to detect the titers of TB-specific IgG and secretory IgA (sIgA) antibodies. Briefly, 96-well flat-bottom polystyrene plates (JETBIOFIL) were coated overnight at 4 °C with 1 μg/mL ESAT-6 or CFP 10 protein diluted in $NaHCO_3$ buffer (pH 9.6). Wells then underwent blocking with 5% BSA for 2 hours at room temperature. After two washes with PBS, serum or lung tissue homogenate samples were added and incubated for 2 h at room temperature to allow specific antigen antibody binding. Following four washes with PBS, the plates were incubated for 3 h at room temperature with HRP-conjugated goat anti-mouse secondary antibodies: IgG (C2225, Applygen; 1:50,000 dilution) or IgA (C2219, Applygen; 1:10,000 dilution). After another four washes with PBS, color was developed using 3,3′,5,5′-tetramethylbenzidine (TMB) substrate. Absorbance was measured at 570 nm with a microplate reader (iMark, Bio Rad), and antibody titers were determined accordingly.

Histological Analysis

For hematoxylin–eosin (H&E) staining, after baking the paraffin sections of the tissue, they were dewaxed with xylene in sequence and hydrated with gradient ethanol. Then, the nuclei were stained with hematoxylin for 5 to 10 minutes, slightly washed with running water, and decomposed with 1% hydrochloric acid ethanol for several seconds, followed by bluing with the bluing solution or running water. The cytoplasm was then stained with eosin for 1 to 3 minutes, dehydrated with gradient ethanol until transparent with xylene, and finally sealed with neutral gum and observed under a microscope. For acid fast staining (AFS), paraffin-embedded lung tissue sections were stained with carbolic acid fuchsin for 15–20 minutes after dewaxing and hydration, decolorized with hydrochloric acid and ethanol, counterstained with methylene blue, and then sealed after dehydration and transparency. Finally, under the light mi-

croscope and oil microscope, the acid-fast staining positive bacteria were bright red, the background was blue, and the image acquisition and analysis were carried out.

Cell Viability Assay

In vitro cytotoxicity of ECQ@PS-LPs was assessed by CCK-8 assay. RAW264.7 cells were seeded into 96-well plates at densities of 5000 and 10,000 cells per well and incubated for 12 h. Following attachment, the medium was replaced with fresh medium containing ECQ@PS-LPs at concentrations of 0, 2, 4, 6, 8, and 10 mg/mL, and cells were incubated for 24 h or 48 h. After treatment, cells were washed three times with PBS, and fresh medium containing 10% CCK-8 reagent was added. Following a 2 h incubation, absorbance was measured at 450 nm using a microplate reader (iMark, Bio-Rad) to determine cell viability.

Statistical Analysis

Most quantitative data are presented as mean ± standard deviation (SD). Differences among multiple groups were analyzed using one-way analysis of variance (ANOVA) followed by post-hoc correction. Statistical analysis was performed using Prism 9.4.1 software (GraphPad Software Inc., San Diego, CA, USA), with $p < 0.05$ considered statistically significant. In this study, except for the microscopic imaging and histological assessment which were conducted in a single-blind manner by the researchers, no blinding was set for the other experiments completed under highly standardized and preset conditions.

Results

Synthesis and Characterization of ECQ@PS-LPs

To prepare ECQ@PS-LPs, 1, 2-dipalmitoyl-sn-glycero-3-phosphate choline (DPPC), 1, 2-dipalmitoyl-sn-glycero-3-phosphate glycerol (DPPG), 1, 2-distearoyl-sn-glycero-3-phosphate ethanolamine-n-[methoxy (polyethylene glycol)-2000] (DSPE-PEG2000) and cholesterol were hydrated using standard lipid membranes to synthesize AS liposomes, encapsulated with M.tb-specific antigens ESAT-6, CFP-10 and adjuvant QS-21, known AS ECQ@PS-LPs. ECQ@PS-LPs were obtained by continuous extrusion of 800 nm, 400 nm, 200 nm polycarbonate filters, which theoretically fuse everything together. It can be seen that ECQ@PS-LPs has the same membrane structure as PS-LPs (Fig. 2**A**, **Supplementary Fig. 1A**). And ESAT-6, CFP-10, QS-21 and PS-LPs were successfully encapsulated on the surface of ECQ@PS-LPs (Fig. 2**B**, **Supplementary Fig. 1B**). The average hydrodynamic size (DLS) of PS-LPs is 190.1 nm, and the average hydrodynamic size (DLS) of ESAT-6, CFP-10 and QS-21-encapsulated liposomes (ECQ@PS-LPs) is 209.2 nm, all around 200 nm (Fig. 2**C**). This size can help the material be absorbed by the tissue more quickly, improving the absorption efficiency of the body. Similarly, Fig. 2**D** shows mean zetas of –7.24 mV and –10.88 mV for PS-LPs and ECQ@PS-LPs, respectively; It has good material stability. To further verify the stability of the material, we measured the average hydrodynamic particle size (DLS) of ECQ@PS-LPs in PBS solution for 7 days, and Fig. 2**E** shows that the particle size of ECQ@PS-LPs in PBS is highly consistent within 7 days, with an average particle size of around 200 nm, which can prove that it is also stable in physiological states. Based on the biological fact that ESAT-6 and CFP-10 form a 1: 1 stable complex (ESAT-6: CFP-10 complex) in a natural environment [28] , we preliminarily assigned the two antigens to 4 μg: 4 μg to mimic their natural conformation, which may be beneficial to the production of more relevant functional antibodies and T cell epitopes; In order to explore the optimal drug loading ratio of QS-21, we set 7 concentration gradients (10, 12, 14, 15, 16, 18, 20) according to the recommended mouse safe dose of QS-21 (10 μg–20 μg) , the results showed that the activation ability of DCs was the strongest at 15 μg, which was dose-dependent, and then there were signs of a slight decrease in cellular activity at a higher ratio, so we chose the ratio of ESAT-6: CFP-10: QS-21 = 4μg: 4μg: 15μg ECQ@PS-LPs formulation group, which performed best on all test indicators (**Supplementary Fig. 2**). To evaluate the encapsulation efficiency, the direct encapsulation efficiency measurement results of CFP-10, ESAT-6 and QS-21 showed that the encapsulation efficiency of the three was about 70% (Fig. 2**F**, **Supplementary Fig. 3**), confirming that this preparation method has good encapsulation for various active ingredients effect.

Capacity of ECQ@PS-LPs for Both Alveolar Surfactant Barrier Penetration and Alveolar Macrophage Uptake

The mouse monocyte/macrophage cell line RAW264.7 is a fundamental model for studying macrophage functions. Under microscopic examination, the undifferentiated M0-state RAW264.7 cells exhibited a round or oval morphology, uniform distribution, consistent size, and were confirmed to be free of mycoplasma contamination (Fig. 3**A**, **Supplementary Fig. 6**). To rigorously authenticate the cell line, we performed flow cytometric analysis following the standards of the International Society for Cell Therapy. The results demonstrated strong positive expression of the characteristic macrophage surface markers CD11b and F4/80 (Fig. 3**B**). In addition, in order to have an immune effect, inhaled vaccines must first be transmitted through the respiratory tract to the alveoli, penetrate pulmonary surfactant (AS), and are absorbed by antigen-presenting cells (APCs) [29]. In order to make our antigen and adjuvant penetrate the AS barrier better, we bind the liposome of biomimetic AS to the antigen and adjuvant. Here, we labeled PS-LPs and ECQ@PS-LPs with fluorescent dye 1, 1-octacoskyl-3, 3, 3, 3-tetramethyldicyanamide iodide (DIR), respectively, and incubated them with RAW264.7 cells for 1 h. Figs. 3**C** and 3**E** show that DIR-labeled ECQ@PS-LPs has the

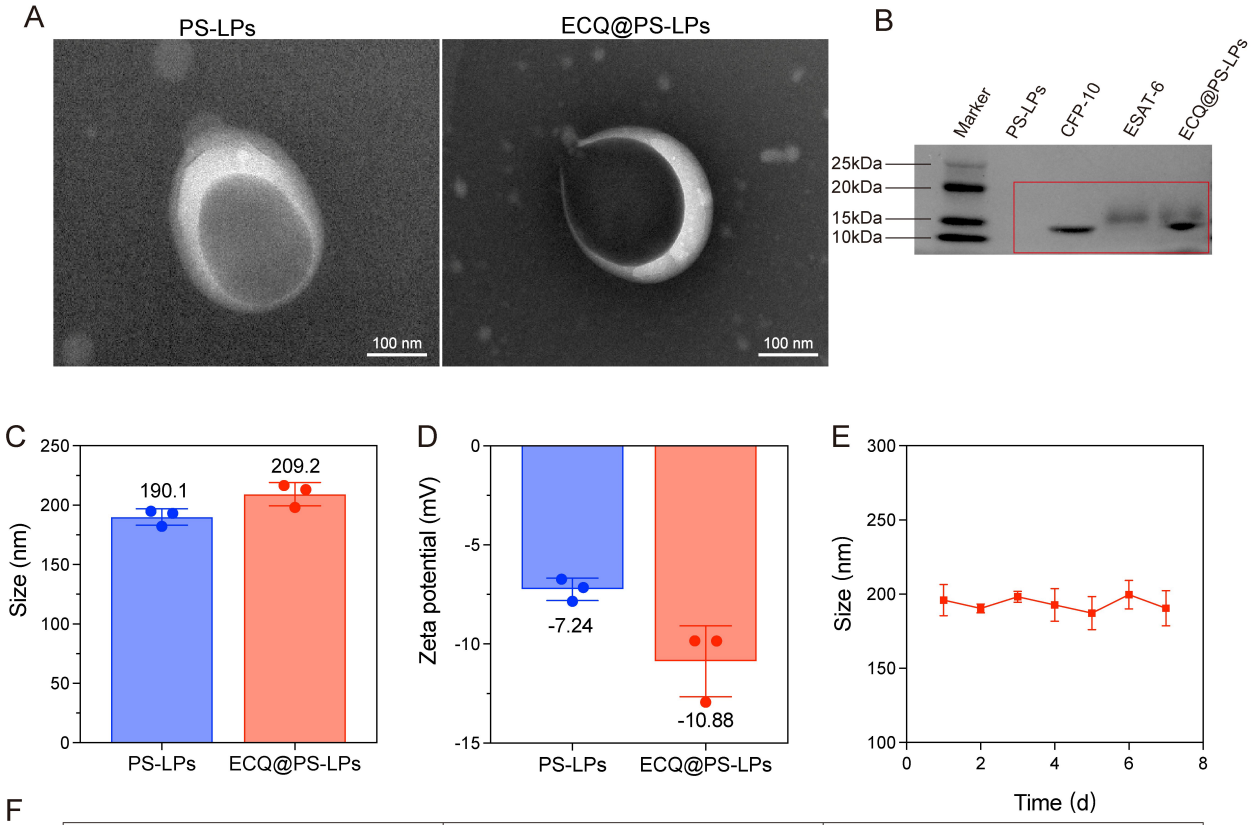

F

Component	Feeding Capacity (μg)	Encapsulation Efficiency (%)
ESAT-6+CFP-10	8	73%± 2.6%
QS-21	15	69% ± 7.2%

Fig. 2. Characterization of ECQ@PS-LPs. (**A**) Representative TEM images of PS-LPs and ECQ@PS-LPs stained with Uranium acetate negative staining. scale bar: 100 nm. (**B**) Proteomic analysis of ECQ@PS-LPs. (**C**) Average hydrodynamic size (DLS) of PS-LPs and ECQ@PS-LPs. (**D**) PS-LPs and ECQ@PS-LPs ζ measurements. (**E**) Average hydrodynamic size (DLS) of ECQ@PS-LPs in PBS over 7 days. (**F**) The encapsulation rate of ESAT-6, CFP-10 and QS-21.

same penetration efficiency AS PS-LPs, which shows that the addition of antigen and adjuvant does not affect the membrane structure, and still has the ability to mimic AS, uptake by antigen-presenting cells, generating a series of immune responses. Likewise, PBS, PS-LPs and ECQ@PS-LPs were dripped into mice through nasal inhalation for 12 h, and the mice were dissected for lung imaging *in vitro*. The fluorescence intensity showed that the two had the same residence ability in the lungs (Figs. 3**D**, 3**F**, and **Supplementary Fig. 4**). In addition, we evaluated the pharmacokinetic behavior of ECQ@PS-LPs *in vivo* (**Supplementary Fig. 5**). The results show that the preparation has significant lung residence characteristics and can maintain an effective concentration in lung tissue for a long time. It mainly metabolically metastasizes to the liver at about 72 hours, and basically completes systemic clearance within 96 hours. It is speculated that it is metabolized from the liver to feces for excretion. It can be proved that ECQ@PS-LPs have the same penetrating ability as PS-LPs both *in vitro* and *in vivo*.

Innate Immune Activation by ECQ@PS-LPs

We evaluated the adjuvant properties of ECQ@PS-LPs by intranasal administration of five different immune

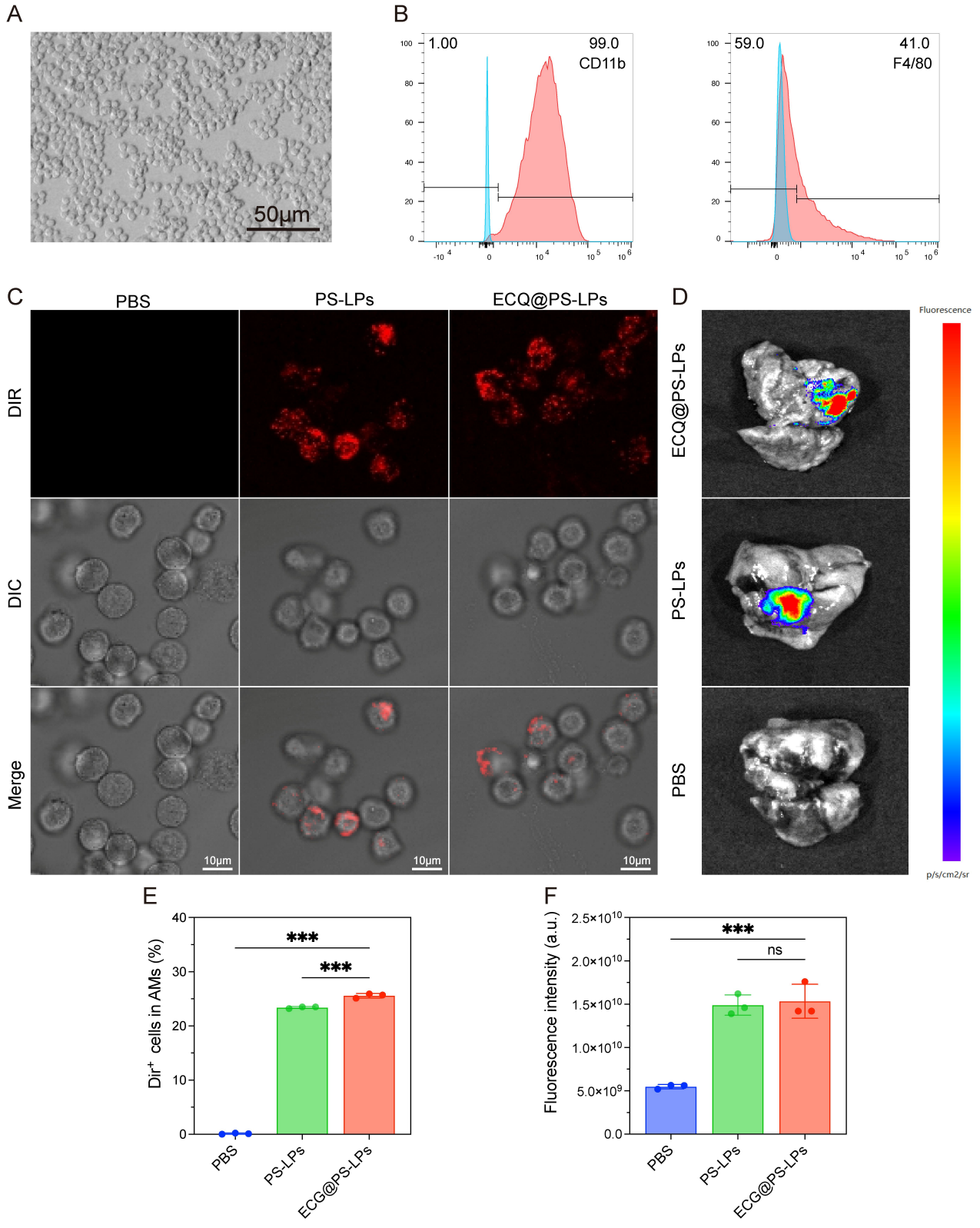

Fig. 3. The Capacity of ECQ@PS-LPs for Both Alveolar Surfactant Barrier Penetration and Alveolar Macrophage Uptake. (**A**) Representative image of RAW264.7 cells. scale bar: 50 μm. (**B**) Characteristic surface markers of RAW264.7 cells assessed by flow cytometry. The blue curve represents the isotype control, and the red curve represents the surface markers on RAW264.7. (**C**) Representative confocal images of RAW264.7 macrophages incubating at 37 °C for 1 hour after phagocytosis of PBS, DIR-labeled PS-LPs, or DIR-labeled ECQ@PS-LPs ($n = 3$). scale bar: 10 μm. (**D**) IVIS imaging of healthy mice 12 hours after intranasal administration of PBS, DIR-labeled PS-LPs, and DIR-labeled ECQ@PS-LPs ($n = 3$). (**E**) Measurement of DIR fluorescence intensity within macrophages shown in Figure A ($n = 3$). (**F**) Intranasal administration of PBS, DIR-labeled PS-LPs, and DIR-labeled ECQ@PS-LPs followed by fluorescence intensity detection in healthy mice 12 hours later ($n = 3$). Data are presented as mean ± SD for Figures C and D. Statistical analysis was performed using one-way ANOVA with appropriate post-hoc tests. Data are presented as $^*p < 0.05$, $^{**}p < 0.01$, $^{***}p < 0.001$.

formulations to healthy mice. After 24 hours, lung tissues were collected for analysis. Flow cytometry was used to determine the percentages of M1-type macrophages and dendritic cell subsets (cDC and mDC). Concurrently, lung tissue homogenates were prepared through grinding and filtration, followed by ELISA to quantify inflammatory cytokines. The experimental groups were designated as follows: G1 (PBS), G2 (free ESAT-6 + CFP-10), G3 (free ESAT-6 + CFP-10 + QS-21), G4 (BCG SC), and G5 (ECQ@PS-LPs), respectively. Figs. 4**A**–4**F**, **Supplementary Fig. 7** show that the antigen-presenting cells (macrophages and dendritic cells) of G2 and G3 groups are significantly different, indicating that after QS-21 binds to ESAT-6 and CFP-10, its immunological effect is greater than ESAT-6 + CFP-10. This is due to the encapsulated QS-21 (full name: Quillaja Saponin 21) is a high-purity saponin molecule extracted from the southern state soapbark tree [21]. It can greatly enhance the immunogenicity of the antigen and produce a stronger and longer-lasting immune response, which is crucial for TB. However, the activation efficiency of ECQ@PS-LPs was significantly higher than that of free antigen-adjuvant preparations. This superior performance is attributed to its unique biomimetic design: the PS-LPs core mimics pulmonary surfactant, enhances lung tissue uptake of encapsulated antigens and adjuvants, and prolongs their retention *in vivo*. The cDCs, mDCs and M1-AMs of ECQ@PS-LPs are 1.23, 1.43 and 1.53 times that of free antigen + adjuvant. (Figs. 4**A**–4**F** and **Supplementary Fig. 7**). Concentration assays of IFN-γ (4**G**), IFN-β (4**H**), and TNF-α (4**I**) in lung tissue showed that ECQ@PS-LPs have the ability to induce the strongest inflammatory response, all indicating that this biomimetic nanovaccine has a strong adjuvant effect. In conclusion, ECQ@PS-LPs have a significant effect on activating innate immune responses.

Specific Immunity Activation Effects of ECQ@PS-LPs

We systematically investigated the mechanisms by which ECQ@PS-LPs induce specific and memory immune activation. As presented in Fig. 5**A**, mice were intranasally vaccinated with ECQ@PS-LPs on day 0 and boosted on day 28. On day 3 after booster immunization, spleen tissue was collected to assess the level of adaptive immunity, including cellular immunity, memory immunity, and mucosal immune responses. M.tb, as a typical intracellular parasite, colonizes mainly host macrophages to evade immune clearance. In the current research and development of TB vaccines, inducing and maintaining a strong cellular immune response is the key to effectively eliminate intracellular bacterial infections. Among them, interferon-γ (IFN-γ) secreted by Th1 cells plays a core regulatory role: it can not only activate infected macrophages, enhance their phagocytolysosomal fusion and respiratory burst capabilities, but also promote nitric oxide synthase The expression of key antibacterial effector molecules, thereby significantly improving the host's clearance efficiency against latent M.tb in cells. The results of Figs. 5**B**, 5**C** and **Supplementary Fig. 8** show that ECQ@PS-LPs can induce a stronger Th1-type immune response compared with free antigen + adjuvant (CFP 10 + ESAT 6 + QS-21), and its response intensity is about 1.8 times that of the free antigen + adjuvant group, G3 is about 1.27 times that of G2; indicating that under the loading of biomimetic nanoparticles, the intracellular killing activity of this vaccine is significantly enhanced. At the same time, Th17 cells also play an important role in defense against extracellular pathogens. By secreting cytokines such as IL-17A, such cells can efficiently recruit neutrophils to the site of infection, enhancing mucosal barrier integrity, it also has synergistic effects with Th1 cells, not only promoting the establishment and maintenance of Th1 immune response, but also indirectly enhancing the clearance of intracellular pathogens such as macrophages by regulating the immune microenvironment. The pattern of immune response induced by ECQ@PS-LPs was significantly different from that of the free antigen + adjuvant group (Figs. 5**D**, 5**E** and **Supplementary Fig. 8**), further confirming that this delivery system can effectively enhance the cellular immune response. Central memory T cells (TCM) are mainly distributed in secondary lymphoid organs such as the spleen. When they encounter pathogens again, they quickly activate, differentiate into effector T cells and migrate to the infected site. ECQ@PS-LPs were able to induce the most significant central immune memory responses (5**F**, 5**G** and **S8**). TRM are usually located in skin lung intestine and other barrier tissues and do not participate in systemic circulation. Since M.tb is mainly transmitted through the respiratory tract, TRM colonized in the lungs can be quickly activated during reinfection, and directly secrete effector molecules to remove the pathogen locally, thus building the first line of defense at the infection gate. Biomimetic nanovaccines can be more efficiently uptake by antigen-presenting cells and induce substantial TRM production in mucosal tissues (Figs. 5**H**, 5**I** and **Supplementary Fig. 8**). Most importantly, ECQ@PS-LPs significantly increased anti-ESAT-6 and anti-CFP-10 IgG antibody titers in the serum of immunized mice (Figs. 5**L**, 5**M**), which can effectively elicit TB-specific humoral immunity. Similarly, ECQ@PS-LPs induced higher levels of ESAT-6-and CFP-10-specific secretory IgA (sIgA) in lung tissue (Figs. 5**J**, 5**K**), a trend consistent with serum IgG responses that generated robust mucosal immunity with potential to prevent respiratory transmission. Notably, ECQ@PS-LPs showed similar immune activation capacity to BCG, but were significantly superior to BCG in inducing sIgA versus IgG responses. To sum up, bionic nanovaccines show significant advantages in cellular immunity, immune memory, and especially mucosal immunity, providing a new strategy for the development of TB vaccines.

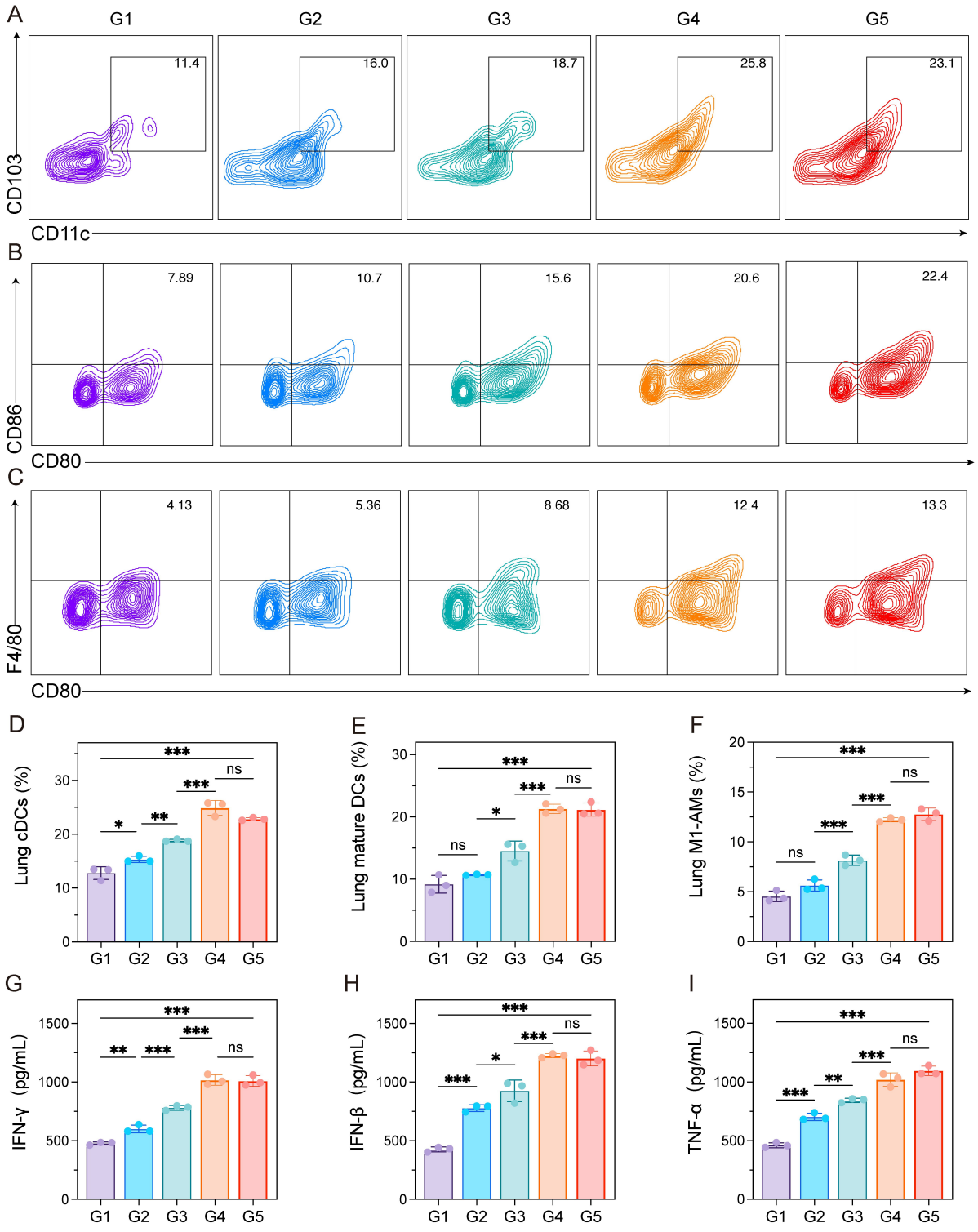

Fig. 4. Innate immune activation effects of ECQ@PS-LPs. (**A**) Representative flow cytometric analysis images of total cDCs (CD11c+CD103+) in alveolar macrophages (AMs) from healthy mice 24 h post-intranasal challenge. (**B**) Representative flow cytometric analysis images of total mDCs (CD11c+CD80+CD86+) in alveolar macrophages (AMs) from healthy mice 24 h post-intranasal challenge. (**C**) Representative flow cytometric analysis images of total M1 macrophages (CD11c+F4/80+CD80+) in alveolar macrophages (AMs) from healthy mice 24 h post-intranasal challenge. (**D**) relative quantification images of cDC (CD11c+CD103+) cells in lung tissue. (**E**) relative quantification images of mDC (CD11c+CD86+CD80+) cells in lung tissue. (**F**) relative quantification images of M1 macrophages (CD11c+F4/80+CD80+) in lung tissue. (**G**) Secretion levels of IFN-γ in lung tissue from healthy mice 24 h post-intranasal challenge. (**H**) Secretion levels of IFN-β in lung tissue from healthy mice 24 h post-intranasal challenge. (**I**) Secretion levels of TNF-α in lung tissue from healthy mice 24 h post-intranasal challenge. G1: PBS; G2: Free antigen (ESAT-6+CFP-10); G3: Free antigen + adjuvant group (ESAT-6 + CFP-10 + QS-21); G4: BCG SC; G5: ECQ@PS-LPs. SC: subcutaneous injection. In panels D-I, data are presented as mean ± SD (n = 3). Post-hoc corrected one-way ANOVA was used to calculate statistical significance. *$p < 0.05$, **$p < 0.01$, ***$p < 0.001$.

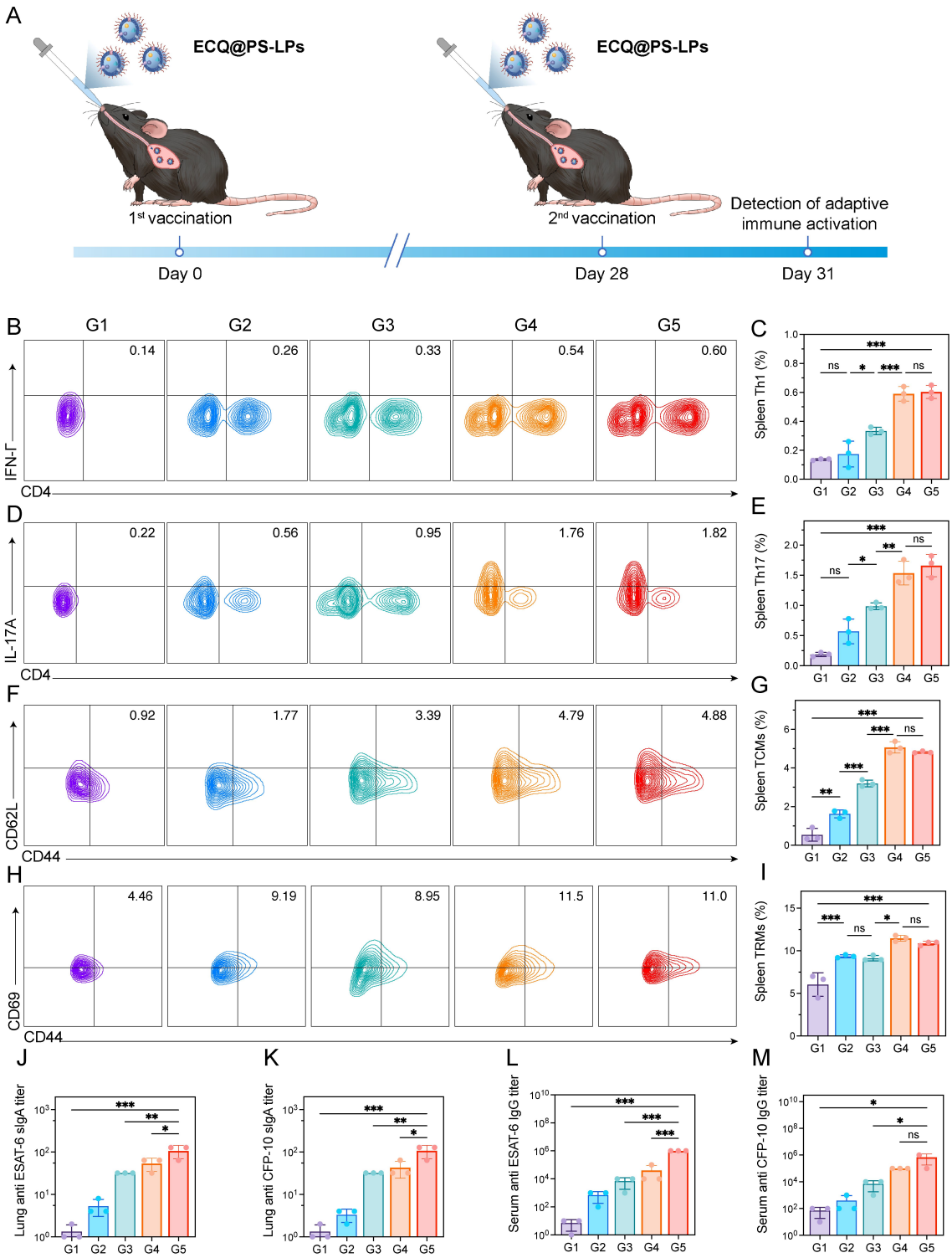

Fig. 5. Specific immunity activation effects of ECQ@PS-LPs. (**A**) Vaccination flowchart and subsequent experiments. (**B**) Flow cytometry analysis images of Th1 (CD3+CD4+IFN-γ+) cells in spleen tissue. (**C**) relative quantification images of Th1(CD3+CD4+IFN-γ) cells in spleen tissue. (**D**) Flow cytometry analysis images of Th17 (CD3+CD4+IL-17A+) cells in spleen tissue. (**E**) relative quantification images of Th17(CD3+CD4+IL-17A) cells in spleen tissue. (**F**) Flow cytometry analysis images of TCM (CD3+CD44+CD62L+) cells in spleen tissue. (**G**) relative quantification images of TCM (CD3+CD44+CD62L+) cells in spleen tissue. (**H**) Flow cytometry analysis images of TRM (CD3+CD44+CD69+) cells in spleen tissue. (**I**) relative quantification images of TRM (CD3+CD44+CD69+) cells in spleen tissue. (**J**) antigen-specific pulmonary sIgA titers of ESAT-6 following immunization in mice. (**K**) antigen-specific pulmonary sIgA titers of CFP-10 following immunization in mice. (**L**) antigen-specific serum IgG titers of ESAT-6 following immunization in mice. (**M**) antigen-specific serum IgG titers of CFP-10 following immunization in mice. G1: PBS; G2: Free antigen (ESAT-6+CFP-10); G3: Free antigen + adjuvant group (ESAT-6 + CFP-10 + QS-21); G4: BCG SC; G5: ECQ@PS-LPs. SC: subcutaneous injection. Data in C, E, G, I and J-M are presented as mean ± SD ($n = 3$). Statistical significance was assessed by one-way ANOVA followed by post-hoc correction. *$p < 0.05$, **$p < 0.01$, ***$p < 0.001$.

Prophylactic Effect of ECQ@PS-LPs

In order to comprehensively evaluate the effect of ECQ@PS-LPs on the prevention of M.tb infection, we selected the BCG strain as a substitute strain for M.tb H37Rv in the absence of a tertiary biosafety laboratory. Challenge experiments were performed on post-immunized mice. The experimental process is shown in Fig. 6**A**, healthy mice were inoculated with different types of vaccines intranasally, the primary immunization was completed on day 0, and the booster immunization was performed on day 28. At the tenth week, the mice were challenged with BCG by nasal inhalation. At the 14th week, the mice were sacrificed. The lung tissues were collected for colony forming unit (CFU) count, H&E staining and acid-fast staining. The results are shown in Fig. 6**B**. Among all experimental groups, the PBS control group had the highest bacterial load in lung tissue. Intrapulmonary CFU counts were significantly lower in the ECQ@PS-LPs immunized group than in the PBS group, with statistically significant differences. In addition, the CFU of the free antigen group was higher than that of the free antigen combined adjuvant group, indicating that QS-21 played a key adjuvant role in this system; The results of acid-fast staining and H&E staining of lung tissue (Fig. 6**C**) further showed that the pathological change trend was consistent with the CFU count results, which jointly verified the above conclusions.

Biosafety Assessment of ECQ@PS-LPs

In any experiment, biosafety is fundamental to all experiments, and we performed safety tests on ECQ@PS-LPs separately *in vivo* and *in vitro*. *In vitro*, RAW264.7 cells were co-incubated with high concentrations of ECQ@PS-LPs (10 mg/mL) for 24 h and 48 h, and did not show cytotoxicity, which was not significantly different from that of the PBS group (Fig. 7**A** and 7**B**). In addition, after a high concentration of ECQ@PS-LPs (10 mg/mL) was incubated with blood cells at 37 °C for 1 hour, the supernatant was taken to measure its absorbance at 576 nm of a microplate reader, PBS was used as a negative control, and ddH_2O was used as a positive control. It can be seen from the figure that at an ECQ of 10 mg/mL, no cytolysis occurs (Fig. 7**C**). *In vivo*, mice were sacrificed after 30 days of nasal inhalation of PBS, ECQ@PS-LPs. Peripheral blood and organ samples were collected for complete blood count, blood biochemistry, and histopathological analysis to evaluate systemic and tissue-level effects. The results showed that no matter whether it was red blood cells, white blood cells, platelets, hemoglobin, or glutamic-pyruvic aminotransferase (ALT), aspartate aminotransferase (AST), creatinine (CREA) and blood urea nitrogen (BUN), there were

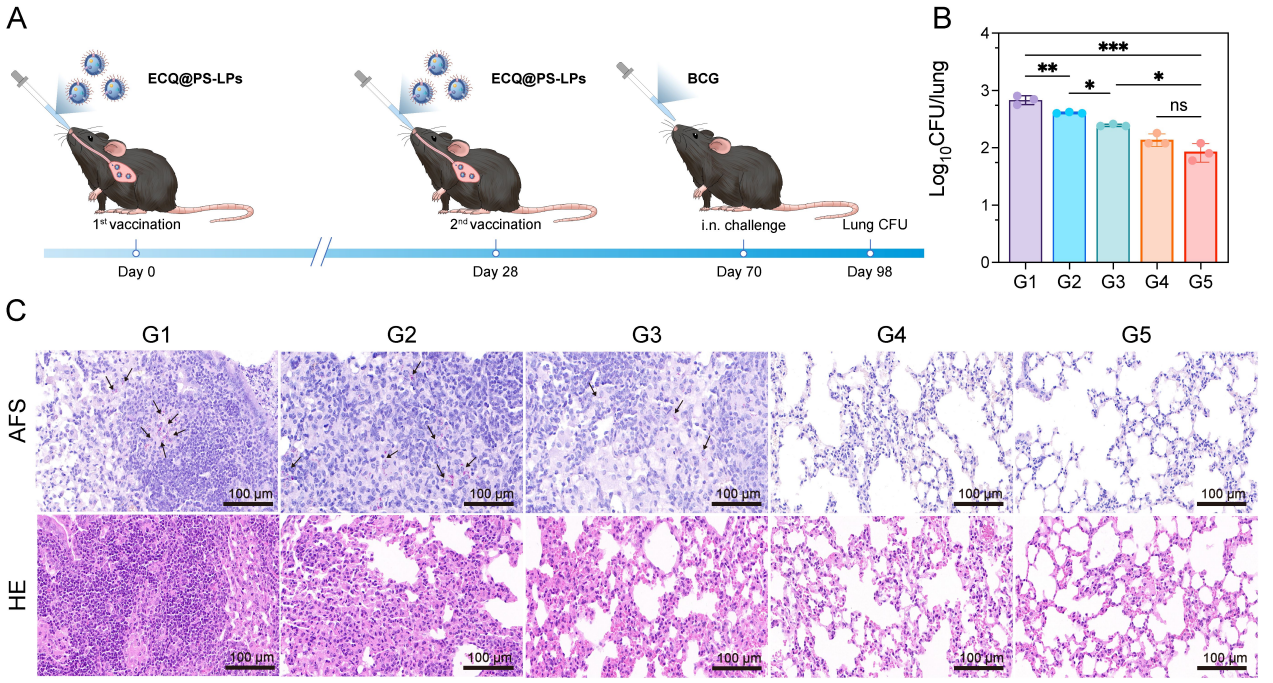

Fig. 6. Comparative Evaluation of Short-Term Protection Against Primary TB Infection Across Administration Protocols. (**A**) Experimental schedule for vaccination and M. tb challenge. (**B**) At the 14th week, bacterial load in the lung of different groups was enumerated and shown as Log10 CFU/organ of individual animals ($n = 3$). (**C**) Representative lung pathology is shown by H&E and acid-fast (AF) staining. ($n = 3$). scale bar: 100 μm. G1: PBS; G2: Free antigen (ESAT-6+CFP-10); G3: Free antigen + adjuvant group (ESAT-6 + CFP-10 + QS-21); G4: BCG SC; G5: ECQ@PS-LPs. SC, subcutaneous injection; H&E, hematoxylin-eosin; AFS, acid-fast staining. Arrows indicated AF-positive bacteria. Statistical significance was assessed by one-way ANOVA followed by post-hoc correction. *$p < 0.05$, **$p < 0.01$, ***$p < 0.001$.

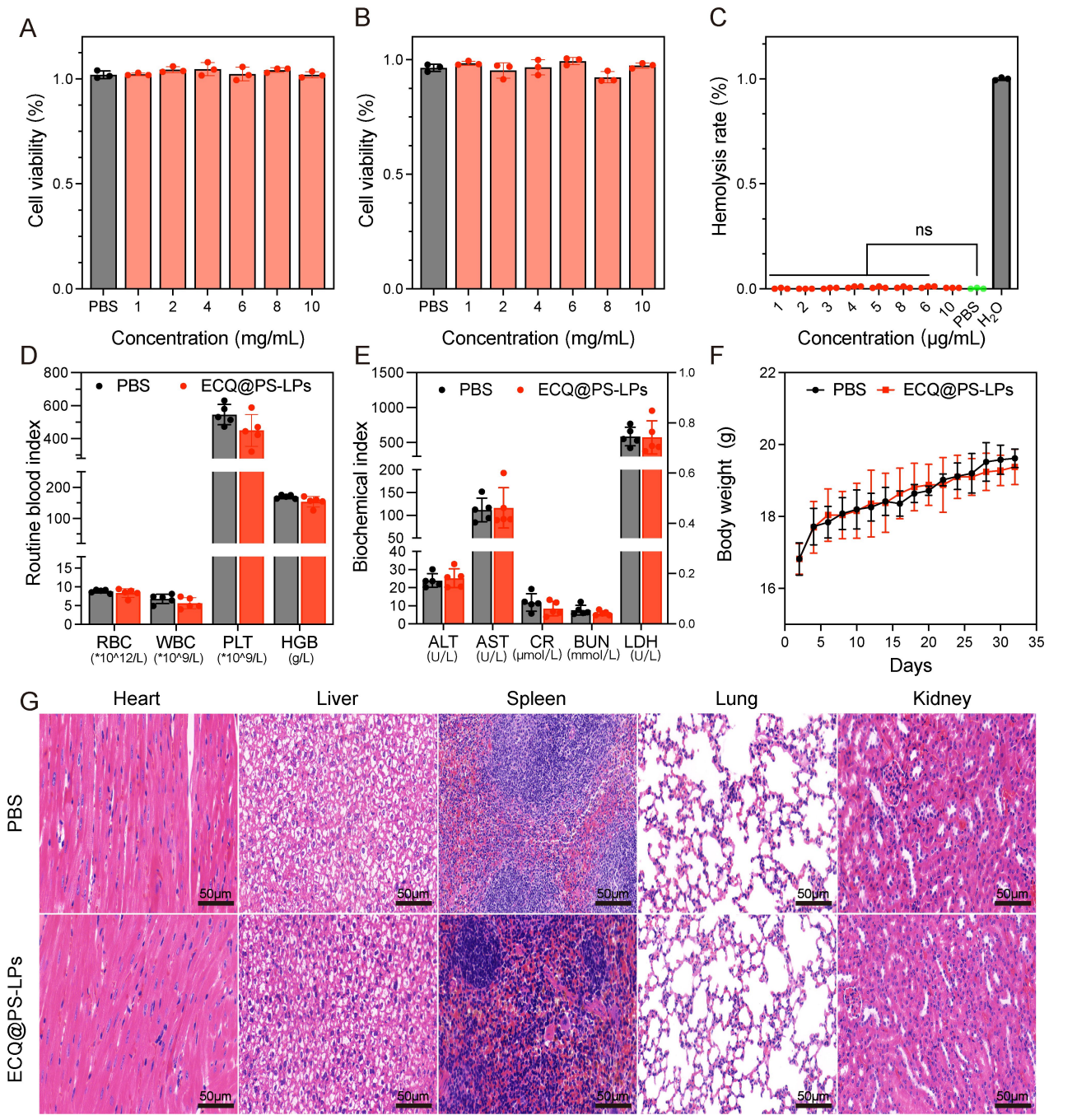

Fig. 7. Preliminary biosafety assessment of ECQ@PS-LPs. (**A**) High concentrations of ECQ@PS-LPs did not induce cell death in normal cells (RAW264.7 cell line) at 24 h (n = 3). (**B**) High concentrations of ECQ@PS-LPs did not induce cell death in normal cells (RAW264.7 cell line) at 48 h (n = 3). (**C**) High concentrations of ECQ@PS-LPs did not cause hemolysis (n = 3). (**D**) Intranasal instillation of high-concentration ECQ@PS-LPs did not cause abnormalities in blood counts (n = 5). (**E**) Intranasal instillation of high-concentration ECQ@PS-LPs did not cause abnormalities in blood biochemistry (n = 5). (**F**) Intranasal instillation of high-concentration ECQ@PS-LPs did not cause body weight loss (n = 5). (**G**) Intranasal instillation of high-concentration ECQ@PS-LPs did not cause abnormalities in major organ damage (n = 5) (scale bar: 50μm), data are displayed as means ± SD.

no significant differences, showing good biological safety (Figs. 7**D** and 7**E**). In addition, 30 days after vaccination, no significant organ toxicity was observed in healthy mice (Fig. 7**G**) Similarly, we tested the body weight of mice, and the body mass index of mice in different groups within 30 days, the PBS group and the experimental group there was no significant difference in mice, and the body weight increased gently (Fig. 7**F**).

Discussion

At present, although a variety of TB vaccines have entered the clinical stage [30], such as MTBVAC [31], VPM1002 [32], M72/AS01E [33], H56: IC31 [34], treatment options for TB are also emerging one after another [35]. there is still a lack of new vaccines with both safety and high efficacy in clinical practice. In view of the rapid development and unique advantages of nanometer materials [36,37], we designed and built a biomimetic nanovaccine ECQ@PS-LPs. Compared with the mixed group using only free adjuvants and antigens, the vaccine exhibited a significantly enhanced immune response, effectively activating systemic cellular immunity and inducing durable immune memory, further validating the advantages of nanodelivery systems. Due to its adoption of the AS bionic nanoparticle system, which mimics pulmonary surfactants, in mice, PS-LPs enters alveolar macrophages (AMs) together with lung-specific surfactant protein-A (SP-A) and protein-D (SP-D). Because it is similar to PS, its goods can be released into the cytoplasm. Then it enters the alveolar epithelial cells (AEC) from the AM through the interstitial junction, and the alveolar epithelial barrier will not be damaged. Although the details of this mechanism are not discussed in depth in this paper, it will be the focus of subsequent research. In addition, compared with subcutaneous BCG, inhaled ECQ@PS-LPs can induce higher levels of specific IgG antibodies in the systemic circulation, and more importantly, can stimulate significant type IgA in the respiratory mucosa (sIgA) response, thereby establishing more effective immune protection in the first line of defense of infection. The preparation process of the vaccine is relatively simple, and it has shown good biosafety in preclinical evaluation, which provides support for its subsequent clinical transformation. ECQ@PS-LPs exhibited better targeted delivery efficiency and stronger T cell activation capacity at the same antigen load compared to other recently reported nanovaccine systems. Especially in inducing local immune memory in the lung, its performance is better than most reported TB vaccine candidates based on liposomes [38] or polymer vectors [39], which is attributed to the AS biomimetic system that effectively promotes vaccine delivery and uptake *in vivo*. However, the TB vaccine still faces many challenges [40]. At present, there is no clear marker related to immune protection. Neither specific antibody titers, T cell numbers, nor cytokine profiles can accurately predict the protective efficacy of vaccines, resulting in the need to pass time-consuming and costly Phase III clinical trials. To verify its validity. In addition, existing animal models can only partially simulate the complex pathological process of human TB, limiting the predictive value of preclinical data. Despite the bottlenecks described above, ECQ@PS-LPs have demonstrated encouraging immunogenicity and safety in preclinical studies, highlighting its translational potential as a novel TB vaccine candidate and deserving further advancement to clinical stage evaluation.

Conclusions

To sum up, the bionic nanovaccine in this study successfully simulated natural pulmonary surfactant, significantly improving its ability to penetrate the lung surface barrier and be absorbed by the mouse body. The inhalable vaccine induced comprehensive immune protection against M.tb. It effectively established mucosal immunity through heightened sIgA levels, while also activating broad-spectrum systemic immunity, including innate responses and adaptive Th1/Th17 polarization alongside elevated antigen-specific IgG. Most importantly, the vaccine induced a strong immune memory effect (manifested as an increase in TCM and TRM cells), thus providing durable and robust protective immunity to mice. All in all, given its high safety and efficacy profile, this vaccine demonstrates great potential for clinical development.

List of Abbreviations

TB, Tuberculosis; M.tb, *Mycobacterium tuberculosis*; BCG, Bacillus Calmette-Guérin; Th1, T helper 1 cell; Th17, T helper 17 cell; TCM, Central memory T cell; TRM, Tissue-resident memory T cell; WHO, World Health Organization; AIDS, Acquired Immunodeficiency Syndrome; HIV, Human Immunodeficiency Virus; MDR, Multidrug-Resistant; XDR, Extensively Drug-Resistant; APCs, Antigen-Presenting Cells; PS, Pulmonary Surfactant; CFU, Colony Forming Unit; AMs, Alveolar Macrophages; H&E, hematoxylin-eosin; AFS, acid-fast staining; SP-A, Surfactant Protein-A; SP-D, Surfactant Protein-D; AEC, Alveolar Epithelial Cells.

Availability of Data and Materials

Data and materials supporting the conclusions of this article are available from the corresponding authors upon reasonable request. Detailed protocols and raw data will be shared promptly with qualified researchers for reproducibility purposes.

Author Contributions

YQW contributed to writing—original draft, project administration, data curation. WFM contributed to supervision, resources. HD and XTF contributed to writing—Methodology, Investigation, Formal analysis. JMW and CHY contributed to supervision, methodology, formal analysis and data curation. QG and YJ contributed to methodology, investigation, data curation. YLZ contributed to visualization, software, investigation. ZHW and FM contributed to validation and investigation. BHR, QQW and YHH contributed to validation, data curation. QM contributed to funding acquisition, supervision. BL contributed to writing—review & editing, resources, funding acquisition, conceptualization. All authors read and ap-

proved the final manuscript. All authors agree to be accountable for all aspects of the work in ensuring that questions related to the accuracy or integrity of any part of the work are appropriately investigated and resolved.

Ethics Approval and Consent to Participate

The research protocol was approved by the Ningxia Medical University Ethics Committee and complied with relevant ethical standards (Approval No.: 2024-G048).

Acknowledgments

Special thanks to Changting He and Yongli Wang for their specific help and useful discussions in the implementation of the experiment and data analysis.

Funding

This work was supported by National Natural Science Foundation of China (82402136), Key Research and Development Program of Ningxia Hui Autonomous Region (2026BEG02026), Natural Science Foundation of Ningxia - Outstanding Youth Program (2024AAC05061), Key Research and Development Program of Ningxia Hui Autonomous Region - Talent Introduction Special Project (2025BEH04084), Chinese College Student Innovation and Entrepreneurship Training Program (202510752021), Open Competition Mechanism to Select the Best Candidates for Key Research Projects of Ningxia Medical University (XJKF230122).

Conflict of Interest

The authors declare no conflict of interest.

Supplementary Material

Supplementary material associated with this article can be found, in the online version, at https://doi.org/10.22203/eCM.v057a03.

References

[1] Natarajan A, Beena PM, Devnikar AV, Mali S. A systemic review on tuberculosis. Indian Journal of Tuberculosis. 2020; 67: 295–311. https://doi.org/10.1016/j.ijtb.2020.02.005.

[2] Carrol ED, Clark JE, Cant AJ. Non-pulmonary tuberculosis. Paediatric Respiratory Reviews. 2001; 2: 113–119. https://doi.org/10.1053/prrv.2000.0118.

[3] Riccardi N, Occhineri S, Vanino E, Antonello RM, Pontarelli A, Saluzzo F, *et al*. How We Treat Drug-Susceptible Pulmonary Tuberculosis: A Practical Guide for Clinicians. Antibiotics (Basel, Switzerland). 2023; 12: 1733. https://doi.org/10.3390/antibiotics12121733.

[4] Glaziou P, Sismanidis C, Floyd K, Raviglione M. Global epidemiology of tuberculosis. Cold Spring Harbor Perspectives in Medicine. 2014; 5: a017798. https://doi.org/10.1101/cshperspect.a017798.

[5] Peddireddy V, Doddam SN, Ahmed N. Mycobacterial Dormancy Systems and Host Responses in Tuberculosis. Frontiers in Immunology. 2017; 8: 84. https://doi.org/10.3389/fimmu.2017.00084.

[6] Kim M, Johnson CE, Schmalstig AA, Annis A, Wessel SE, Van Horn B, *et al*. A long-acting formulation of rifabutin is effective for prevention and treatment of Mycobacterium tuberculosis. Nature Communications. 2022; 13: 4455. https://doi.org/10.1038/s41467-022-32043-3.

[7] Schito M, Migliori GB, Fletcher HA, McNerney R, Centis R, D'Ambrosio L, *et al*. Perspectives on Advances in Tuberculosis Diagnostics, Drugs, and Vaccines. Clinical Infectious Diseases. 2015; 61 Suppl 3: S102–S118. https://doi.org/10.1093/cid/civ609.

[8] Mangtani P, Abubakar I, Ariti C, Beynon R, Pimpin L, Fine PE, *et al*. Protection by BCG vaccine against tuberculosis: a systematic review of randomized controlled trials. Clinical Infectious Diseases. 2014; 58: 470–480. https://doi.org/10.1093/cid/cit790.

[9] Martinez L, Cords O, Liu Q, Acuna-Villaorduna C, Bonnet M, Fox GJ, *et al*. Infant BCG vaccination and risk of pulmonary and extrapulmonary tuberculosis throughout the life course: a systematic review and individual participant data meta-analysis. The Lancet Global Health. 2022; 10: e1307–e1316. https://doi.org/10.1016/s2214-109x(22)00283-2.

[10] Gröschel MI, Prabowo SA, Cardona PJ, Stanford JL, van der Werf TS. Therapeutic vaccines for tuberculosis–a systematic review. Vaccine. 2014; 32: 3162–3168. https://doi.org/10.1016/j.vaccine.2014.03.047.

[11] Ullah I, Bibi S, Ul Haq I, Safia, Ullah K, Ge L, *et al*. The Systematic Review and Meta-Analysis on the Immunogenicity and Safety of the Tuberculosis Subunit Vaccines M72/AS01(E) and MVA85A. Frontiers in Immunology. 2020; 11: 1806. https://doi.org/10.3389/fimmu.2020.01806.

[12] Hu Z, Lu SH, Lowrie DB, Fan XY. Research Advances for Virus-vectored Tuberculosis Vaccines and Latest Findings on Tuberculosis Vaccine Development. Frontiers in Immunology. 2022; 13: 895020. https://doi.org/10.3389/fimmu.2022.895020.

[13] Vidal SJ, Lasrado N, Tostanoski LH, Chaudhari J, Mbiwan ER, Neka GD, *et al*. Mining the CD4 antigen repertoire for next-generation tuberculosis vaccines. Cell. 2025; 188: 6791–6803.e6713. https://doi.org/10.1016/j.cell.2025.08.027.

[14] Li Z, Wang Y, Mo F, Wolter T, Hong R, Barrett A, *et al*. Engineering pyroptotic vesicles as personalized cancer vaccines. Nature Nanotechnology. 2025; 20: 1108–1118. https://doi.org/10.1038/s41565-025-01931-2.

[15] Wang J, Zhang Y, Jia Y, Xing H, Xu F, Xia B, *et al*. Targeting vaccines to dendritic cells by mimicking the processing and presentation of antigens in xenotransplant rejection. Nature Biomedical Engineering. 2025; 9: 201–214. https://doi.org/10.1038/s41551-025-01343-6.

[16] You Q, Wu G, Li H, Liu J, Cao F, Ding L, *et al*. A nanovaccine targeting cancer stem cells and bulk cancer cells for postoperative cancer immunotherapy. Nature Nanotechnology. 2025; 20: 1298–1311. https://doi.org/10.1038/s41565-025-01952-x.

[17] Suo M, Shangguan P, Deng S, Liu Y, Wu K, Ning S, *et al*. Facilitating direct presentation of tumor antigens to activate anti-tumor immunity by phototherapy-potentiated hybrid vaccine. Materials Today. 2025; 90: 270–284. https://doi.org/10.1016/j.mattod.2025.09.025.

[18] Wu J, Ma G. Imitation of nature: Bionic design in the study of particle adjuvants. Journal of Controlled Release. 2019; 303: 101–108. https://doi.org/10.1016/j.jconrel.2019.04.004.

[19] Song J, Wang M, Zhou L, Tian P, Sun Z, Sun J, *et al*. A candidate nanoparticle vaccine comprised of multiple epitopes of the African swine fever virus elicits a robust immune response. Journal of Nanobiotechnology. 2023; 21: 424. https://doi.org/10.1186/s12951-023-02210-9.

[20] Passos BBS, Araújo-Pereira M, Vinhaes CL, Amaral EP, Andrade BB. The role of ESAT-6 in tuberculosis immunopathology. Frontiers in Immunology. 2024; 15: 1383098. https://doi.org/10.3389/fimmu.2024.1383098.

[21] Hu Y, Wu Y, Liu H, Cheng S, Wen F, Wan L. QS–21: Structural insights, immunological mechanisms, and prospects for rational design of safer vaccine adjuvants. European Journal of Medici-

nal Chemistry. 2026; 301: 118223. https://doi.org/10.1016/j.ejmech.2025.118223.
[22] Mettelman RC, Allen EK, Thomas PG. Mucosal immune responses to infection and vaccination in the respiratory tract. Immunity. 2022; 55: 749–780. https://doi.org/10.1016/j.immuni.2022.04.013.
[23] Renukaradhya GJ, Narasimhan B, Mallapragada SK. Respiratory nanoparticle-based vaccines and challenges associated with animal models and translation. Journal of Controlled Release. 2015; 219: 622–631. https://doi.org/10.1016/j.jconrel.2015.09.047.
[24] Lyadova IV, Panteleev AV. Th1 and Th17 Cells in Tuberculosis: Protection, Pathology, and Biomarkers. Mediators of Inflammation. 2015; 2015: 854507. https://doi.org/10.1155/2015/854507.
[25] Schenkel JM, Masopust D. Tissue-resident memory T cells. Immunity. 2014; 41: 886–897. https://doi.org/10.1016/j.immuni.2014.12.007.
[26] Sallusto F, Geginat J, Lanzavecchia A. Central memory and effector memory T cell subsets: function, generation, and maintenance. Annual Review of Immunology. 2004; 22: 745–763. https://doi.org/10.1146/annurev.immunol.22.012703.104702.
[27] Shi T, Ye Y, Fan Z, Yang Q, Ma Y, Zhu J. Respiratory mucosal vaccines: Applications, delivery strategies and design considerations. Biomedicine & Pharmacotherapy. 2025; 189: 118326. https://doi.org/10.1016/j.biopha.2025.118326.
[28] Renshaw PS, Lightbody KL, Veverka V, Muskett FW, Kelly G, Frenkiel TA, *et al*. Structure and function of the complex formed by the tuberculosis virulence factors CFP-10 and ESAT-6. EMBO Journal. 2005; 24: 2491–2498. https://doi.org/10.1038/sj.emboj.7600732.
[29] Hamilos DL. Antigen presenting cells. Immunological Research. 1989; 8: 98–117. https://doi.org/10.1007/bf02919073.
[30] Bouzeyen R, Javid B. Therapeutic Vaccines for Tuberculosis: An Overview. Frontiers in Immunology. 2022; 13: 878471. https://doi.org/10.3389/fimmu.2022.878471.
[31] Lacámara S, Martin C. MTBVAC: A Tuberculosis Vaccine Candidate Advancing Towards Clinical Efficacy Trials in TB Prevention. Archives of Bronconeumology. 2023. https://doi.org/10.1016/j.arbres.2023.09.009.
[32] Nieuwenhuizen NE, Kulkarni PS, Shaligram U, Cotton MF, Rentsch CA, Eisele B, *et al*. The Recombinant Bacille Calmette-Guérin Vaccine VPM1002: Ready for Clinical Efficacy Testing. Frontiers in Immunology. 2017; 8: 1147. https://doi.org/10.3389/fimmu.2017.01147.
[33] Ottenhoff THM. A Trial of M72/AS01E Vaccine to Prevent Tuberculosis. New England Journal of Medicine. 2020; 382: 1576–1577. https://doi.org/10.1056/NEJMc2001364.
[34] Borges ÁH, Russell M, Tait D, Scriba TJ, Nemes E, Skallerup P, *et al*. Immunogenicity, safety, and efficacy of the vaccine H56:IC31 in reducing the rate of tuberculosis disease recurrence in HIV-negative adults successfully treated for drug-susceptible pulmonary tuberculosis: a double-blind, randomised, placebo-controlled, phase 2b trial. The Lancet Infectious Diseases. 2025; 25: 751–763. https://doi.org/10.1016/s1473-3099(24)00814-4.
[35] Wang H, Li X, Li P, Feng Y, Wang J, Gao Q, *et al*. Uptake of Biomimetic Nanovesicles by Granuloma for Photodynamic Therapy of Tuberculosis. ACS Omega. 2025; 10: 6679–6688. https://doi.org/10.1021/acsomega.4c08127.
[36] Huang X, Ma Y, Ma G, Xia Y. Unlocking the Therapeutic Applicability of LNP-mRNA: Chemistry, Formulation, and Clinical Strategies. Research. 2024; 7: 0370. https://doi.org/10.34133/research.0370.
[37] He L, Pan R, Liang R, Li B, Zhang P, He S, *et al*. Nanomaterial Adjuvants for Veterinary Vaccines: Mechanisms and Applications. Research. 2025; 8: 0761. https://doi.org/10.34133/research.0761.
[38] Han Z, Lan YR, Yuan B, Chen QL. Irisin liposomes inhibit ferroptosis and improve atherosclerosis in mouse models via the NRF2/HO-1 signaling pathway. European Cells & Materials. 2025; 54: 16–30. https://doi.org/10.22203/eCM.v054a02.
[39] Liu LY, Zeng FC, He YW, Dong SW, Li JM. Photo-crosslinked hydrogel for enhanced bone defect regeneration via sustained release OGP(10–14). European Cells & Materials. 2026; 55. https://doi.org/10.22203/eCM.v055a02.
[40] An Y, Ni R, Zhuang L, Yang L, Ye Z, Li L, *et al*. Tuberculosis vaccines and therapeutic drug: challenges and future directions. Molecular Biomedicine. 2025; 6: 4. https://doi.org/10.1186/s43556-024-00243-6.

Editor's note: The Scientific Editors responsible for this paper were Pengyuan Wang and Kelong Fan.

Received: 16th October 2025; **Accepted**: 10th March 2026; **Published**: 29th May 2026